Mesoporous structure regulation of activated carbons and effects on the synergistic efficacy of synchronous adsorption and Bio-degradation in biological activated carbon process

Xu-Jin Gong, Yu-Qi Dong and Wei-Guang Li

ABSTRACT

Mesoporous activated carbon MCGL-4 was tailored for simultaneous enhancement of adsorption and bio-degradation by multistage depth-activation (MDA). Synergistic efficacy of synchronous adsorption and bio-degradation was evaluated in pilot-scale bio-enhanced activated carbon (BEAC) system. Results identified that MCGL-4 obtains synchronously well-developed meso- (0.7605 cm^3/g), micro- (0.2655 cm^3/g) and macro-porous (0.143 cm^3/g) structures. Higher volume during 20.4–208.2 Å (0.6848 cm^3/g) ensured higher adsorption capacities for natural organic matters (NOM). The initial immobilized biomass and stabilities on MCGL-4 were also significantly promoted. Rapid small-scale column tests system (RSSCTs) tests showed that adsorption capacities for humic-like organics were 67,725.32 mg·DOC/(kg·carbon) at 39.50 $m^3{\cdot}H_2O$/(kg·carbon). In BEAC system, MCGL-4 achieved higher removal efficiency for fulvic acid, humic acid and aromatic organic matters than commercial carbons. At 39.50 $m^3{\cdot}H_2O$/(kg·carbon), cumulative uptake of organic-pollutants achieved by MCGL-4 was 94,850.51 mg·DOC/(kg·carbon). The proportion occupied by bio-degradation were 31,674.70 mg·DOC/(kg·carbon). It also confirmed that bio-degradation ability was much higher than commercial carbons after mesoporous structures regulation by MDA process.

Key words | activated carbon, adsorption, bio-degradation, bio-enhanced activated carbon (BEAC), natural organic matters, pore-structure regulation

Xu-Jin Gong (corresponding author)
Yu-Qi Dong
School of Energy and Civil Engineering,
Harbin University of Commerce,
Harbin 150090,
China
E-mail: *xujin_gong@126.com*

Wei-Guang Li
School of Environment,
Harbin Institute of Technology,
Harbin 150090,
China

HIGHLIGHTS

- MCGL-4 was tailored for simultaneous bio-enhancement and adsorption by Multistage Depth-Activation.
- MCGL-4 is a promising adsorbent for effective removal of natural organic matters from water.
- MCGL-4 was more conductive to simultaneous biodegradation and adsorption of organic-pollutants.
- Mesopores (20.4 ~ 208.2 Å) played important role in adsorption of humic-like organics.

NOMENCLATURE

KBV	Volume of water treated by per kilogram of activated carbon ($m^3{\cdot}H_2O$/(kg·carbon))	S_{micro}	t-Plot micropore area (m^2/g)
S_{BET}	BET surface area (m^2/g)	V_{total}	Total pore volume (cm^3/g)
		V_{micro}	t-Plot micro-porous volume (cm^3/g)

doi: 10.2166/ws.2020.293

V_{mes}	Calculated mesoporous volume: $V_{mes} = V_{total} - V_{micro}$ (cm^3/g)
$V_{treated}$	Volume of water treated by carbons (m^3)
V_{IN}	Adsorption capacities for iodine(mg/g)
V_{MB}	Adsorption capacities for methylene blue (mg/g)
V_{HA}	Adsorption capacities for humic acid (mg/g)
N	Days of operation (d)
Q_{in}	Flow rate (L/d)
W_{AC}	Weight of carbon in column (kg)
QC	Cumulative uptake of DOC (mg·DOC/(kg·carbon))
Δt_i	Time interval between two sampling dates (d)
DOC_{in}^{i}	Influent DOC at time i (mg/L)
DOC_{out}^{i}	Effluent DOC at time i (mg/L)

INTRODUCTION

Advanced water treatment using activated carbon has been applied worldwide because of the high efficiency and economic performance, such as carbon adsorption (Li *et al.* 2012; Gong *et al.* 2013), ozone-biological activated carbon (O_3-BAC) (Gao *et al.* 2010) and bio-enhanced activated carbon (BEAC) (Zhang *et al.* 2011; Al-Amrani *et al.* 2012). Bio-enhancement in BEAC process ensured higher purification efficiency and service-life (Piai *et al.* 2020). The use of BEAC/BAC for removing natural organic matters and toxic xenobiotics is advisable as the final stage of water purification (Smolin *et al.* 2020). However, tailoring or selecting excellent carbon for BEAC process remains a challenge. The method for the assessment of the contribution of adsorption and bio-degradation in dynamic BEAC/BAC process is also extremely complex (Piai *et al.* 2020; Smolin *et al.* 2020; Ti *et al.* 2020; Zhiteneva *et al.* 2020).

High adsorption capacities for natural organic matter (NOM) and trace organic-pollutants (TrOPs) require synchronously well-developed micro- and meso-porosity distribution of carbons (Gong *et al.* 2020). Studies suggested that meso-pores (2–50 nm) and secondary micro-pores (1–2 nm) principally controlled adsorption of NOM from water (Velten *et al.* 2011). NOM suffered severely competitive adsorption with trace organic-pollutants (TrOPs) on carbon surfaces with primarily small micro-pores (<1.0 nm) (Quinlivan *et al.* 2005). On the other hand, synchronous adsorption and bio-degradation is the core mechanism of organic-pollutants removal in BEAC process (Velten *et al.* 2011; Gibert *et al.* 2012). And it can be significantly affected by pore structure distribution of meso- and macros-pores (Aktaş & Çeçen 2007).

Therefore, tailoring an efficient carbon with a perfect matching between adsorption and bio-degradation (both biomass and bio-activity levels on carbon surfaces) was a significantly important, and pore structure regulation is the promising way to improve adsorption and bio-degradation efficiency simultaneously (Sulaymon *et al.* 2010). Studies suggested that carbons with simultaneously well-developed meso- and micro-porous structures may achieve better matching between adsorption and bio-degradation (Singh *et al.* 2012). However, micro-porous carbons were still commonly employed in drinking water treatment plants (DWTPs) due to the industrialization restriction in China. Research and development of new-type mesoporous carbons was financially supported by the Ministry of Housing and Urban-Rural Development of China in the present work. A series of innovative mesoporous carbons were successfully prepared. However, it is still a challenging work to quantify the effects of pore structure regulation on synergy-effect between bio-degradation and adsorption. Therefore, quantification of adsorption and bio-degradation on new carbons in BEAC/BAC process was also conducted in present work.

MATERIALS AND METHODS

Activated carbon preparation

Three new carbons were prepared by multi-step procedure in Figure 1, including precursor-blending, re-agglomeration, potassium hydroxide (KOH) impregnation, carbonization and multistage depth-activation (MDA) (Li *et al.* 2014; Gong *et al.* 2015a, 2015b). Take carbon MCGL-4 as an example, the detailed preparation parameters were described as the following: coal-blending (35% Taixi coal +30% Shen Fu coal) and coconut shell (30%) were first mixed and crushed to 100–200 mesh. The mixture was agglomerated using refined tar (5%) as agglomerate. The agglomerated material was crushed and screened again to 2–10 mm. Impregnation was conducted before carbonization using 10% KOH (100 rpm, 60 min).

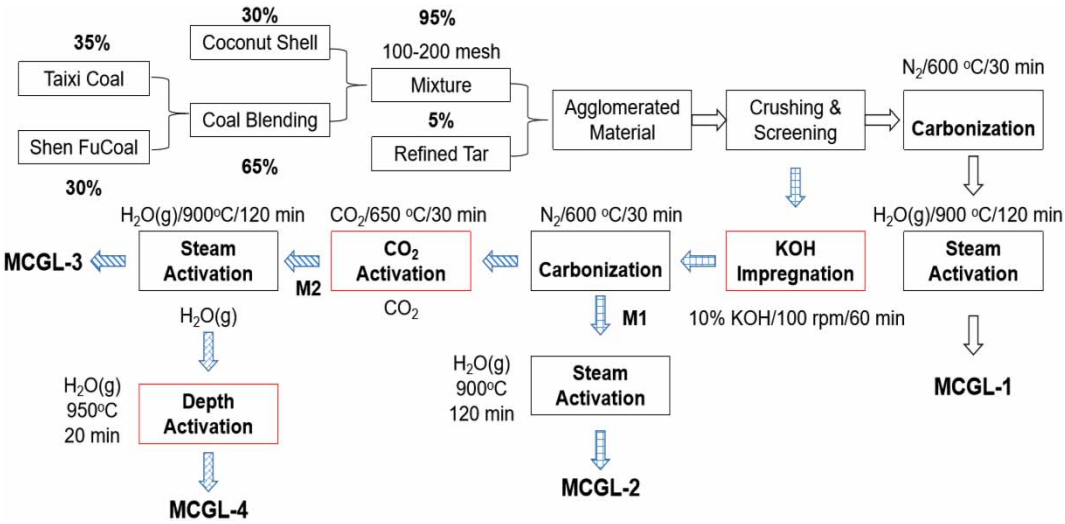

Figure 1 | Preparation procedure of new carbons.

Carbonization was consequently conducted at 600 °C in N_2 protection environment for 30 min. MDA was conducted in activation apparatus, and MDA can be divided into three stages: CO_2 activation (650 °C/30 min), steam activation (900 °C/120 min) and depth-steam activation (950 °C/20 min).

Activated carbon characterization

Nitrogen isotherms were measured by ASAP2020 Sorptometer at 77 K and the specific surface area (S_{BET}) was calculated by Brunauer–Emmett–Teller (BET) model (Praetorius & Voigt 2015; Spiesshofer *et al.* 2015; Wang 2016). Pore size distribution/pore volume distribution (PSDs/PVDs) were calculated by *t*-plot method (Gong *et al.* 2013). Especially, micro-porous volume (V_{micro}) was also identified by Horvath-Kawazoe (H-K) model. Mesoporous volume (BJH-V_{mes}) was calculated by Barrett-Joyner-Halenda (BJH) model (Choi *et al.* 2015; Haluszka *et al.* 2015). Adsorption capacities for iodine (V_{IN}), methylene blue (V_{MB}) and humic acid(V_{HA}) were determined according to the National Standards of China (GB/T 7702.7-2008, 7702.6-2008 and 7701.2-2008).

Commercial carbons

Three kinds of commercial carbons in Table 1 were also employed as control group, which were commonly used in a water purification plant in China.

Table 1 | Parameters of commercial carbons employed in present work

		Commercial carbons		
Parameters	**Unit**	**SX-10**	**F400**	**ZJ15**
Specific surface area (S_{BET})	m^2/g	921	1,169	924
External surface area (S_{Ext})	m^2/g	256.31	–	301.39
Microporous surface area (S_{Micro})	m^2/g	556.09	939.5	519.17
Total pore volume (V_{total})	cm^3/g	0.6536	0.8963	0.3714
Microporous volume (V_{micro})	cm^3/g	0.2390	0.4716	0.2541
Mesoporous volume(V_{mes})	cm^3/g	0.2927	0.3170	0.042
Macroporous volume (V_{mar})	cm^3/g	0.1219	0.1077	0.0753
Average pore diameter (D)	Å	26.98	28.94	18.26

Table 2 | Operational parameters and feed water qualities of PCT and RSSCT system

Parameters	**Pilot system**	**RSSCT system**
Granule size – (mm)	0.60–2.50 (1.50)	0.21
Empty bed contact time (EBCT) (min)	20	0.40
Flow rate (m^3/d)	0.185	0.064
Filtering velocity (m/h)	3.9	27.86
Height (m)	2.10	0.35
Carbon bed depth (m)	1.20	0.24
Column diameter (cm)	5	1.1
Temperature (°C)	15.45 ± 7.93	17.10 ± 3.59
DOC(mg/L)	3.28 ± 0.47	3.20 ± 0.15
UV_{254} (cm^{-1})	0.078 ± 0.015	0.074 ± 0.012
Turbidity (NTU)	0.38 ± 0.16	0.35 ± 0.11

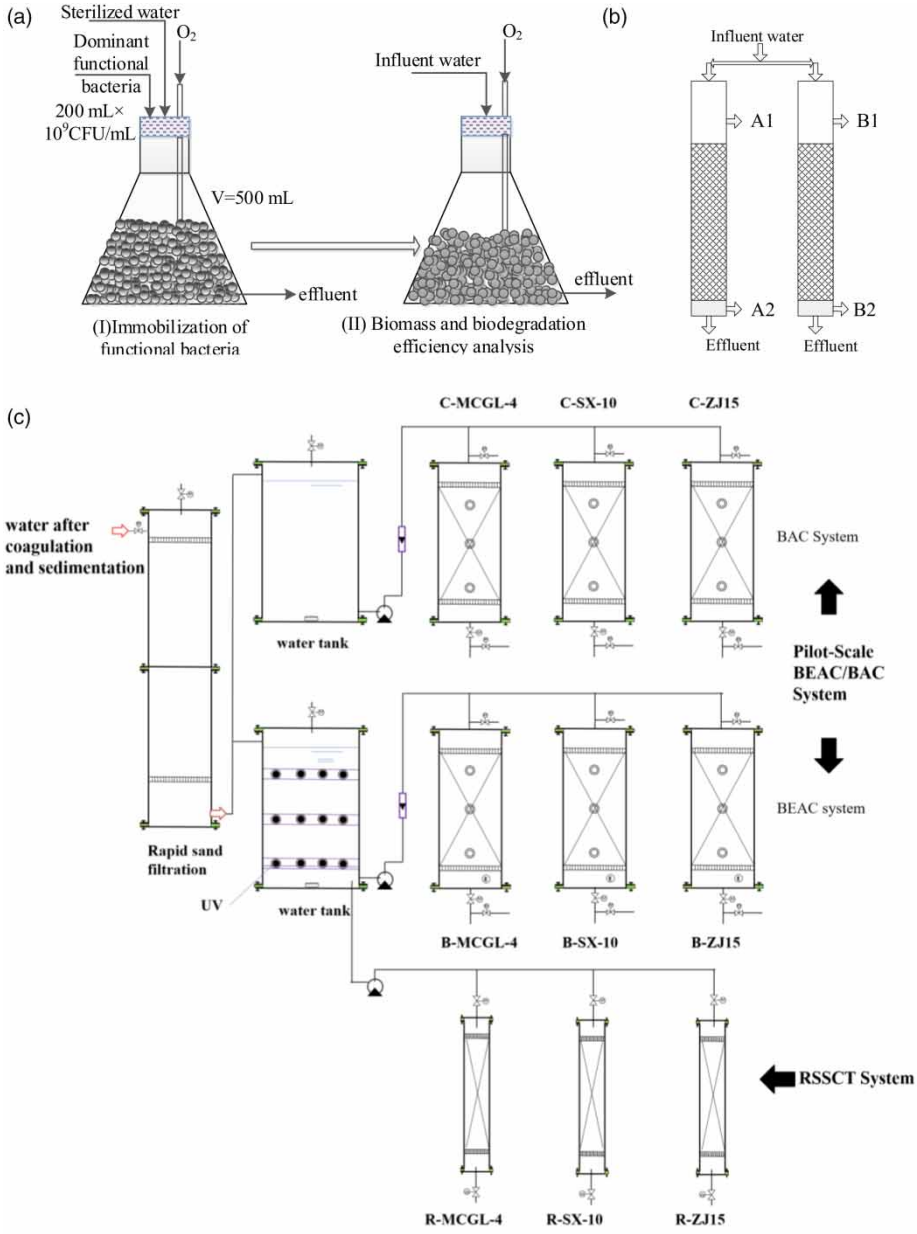

Figure 2 | Experimental set-up. (a) Evaluation set-up for initially immobilized biomass, (b) evaluation set-up for dissolved oxygen utilization, (c) pilot-scale BEAC/BAC system and RSSCT tests system.

Experimental apparatus

Testing apparatus of functional bacteria immobilization

As shown in Figure 2(a), carbons (300 mL) were fixed into conical bottles after steam sterilization, and the empty bed contact time (EBCT) was 30 min. Functional bacteria were enriched from steady BEAC process, mainly contains *Acinetobacter Harbinensis sp.*, three strains of *Pseudomonas sp.* and *Bacillus subtilis*. After fermenting, functional bacteria (10^9 CFU/L) were circularly immobilized onto carbons (24 h). Biomass (phospholipid contents) on different carbons was determined at different times.

Utilization rates of dissolved oxygen (DO) during bio-degradation by different carbons were determined using apparatus in Figure 2(b) in both adsorption system (column A) and bio-enhancement system (column B with functional bacteria immobilization). The influent raw water was sterilized by ultraviolet and fully aerated. Dissolved organic carbon (DOC) and NH_4^+-N were adjusted to 4.0 ± 0.25 mg/L and 0.50 ± 0.16 mg/L, respectively, using sodium acetate and ammonium chloride. After stable operation for a week, changes of DOC, DO and NH_4^+-N were determined for 5 days, using HQ30D portable DO analyzer and TOC analyzer (TOC-VCPH).

Herein, bio-degradation can be ignored in column A and the DOC and NH_4^+-N removal can be attributed to adsorption, rather than bio-degradation. And DO consumption in column A can be defined as ΔDO_{CS} (surface affinity for DO by adsorption process). Therefore, utilization efficiency of DO which was caused by surface bio-degradation in column B can be calculated using as following Equations (1)–(8):

NO.	Equations	Units	Annotation
(1)	$\Delta DO_{CS} = DO_{A1} - DO_{A2}$	mg/L	Surface affinity for DO by adsorption in column A
(2)	$\Delta DOC_{\mathrm{Bio}} = \Delta DOC_B - \Delta DOC_A$	mg/L	DOC removal by bio-degradation in column B
(3)	$\Delta N_{\mathrm{Bio}} = \Delta(NH_4^+ - N)_B - \Delta(NH_4^+ - N)_A$	mg/L	NH_4^+-N removal by bio-degradation in column B
(4)	$\Delta DO_C = 2.66\mathrm{mg} \cdot \mathrm{O_2}/(\mathrm{mg} \cdot DOC) \times \Delta DOC_{\mathrm{Bio}}$	mg/L	Theoretical amount of DO required for DOC degradation
(5)	$\Delta DO_N = 4.33\mathrm{mg} \cdot \mathrm{O_2}/(\mathrm{mg} \cdot NH_4^+ - N) \times \Delta N_{\mathrm{Bio}}$	mg/L	Theoretical amount of DO required for NH_4^+-N degradation
(6)	$\Delta DO_{TH} = \Delta DO_C + \Delta DO_N + \Delta DO_{CS}$	mg/L	Theoretical consumption of DO in column B
(7)	$\Delta DO_R = DO_{B1} - DO_{B2}$	mg/L	Actual consumption of DO in column B
(8)	$PADO = \frac{\Delta DO_C + \Delta DO_N}{\Delta DO_R} \times 100\%$	%	Actual effective utilization rate of DO by bio-degradation

Pilot-scale column testing system (BAC/BEAC process)

As shown in Figure 2(c), pilot-scale BAC/BEAC system (1.0 $m^3 \cdot h^{-1}$) and rapid small-scale column tests system (RSSCTs) were established, treating water from Songhua River. Influent water was pre-treated by coagulation, inclined-tube sedimentation and rapid sand filtration. Pilot-scale BEAC system contains three parallel columns (φ50 mm × 2.10 m), packed with 1.20 m carbon bed and operated in up-flow mode (184 L/d). After enrichment and domestication, cyclic immobilization of the dominant functional in BEAC columns was conducted according to the methods described by Zhang (Zhang *et al.* 2011). Ultraviolet sterilization (100 $W \cdot m^{-2}$) was employed in raw water tank to minimize the bacteria interference. Difference between BAC and BEAC system was the formation of bio-degradation. Bio-degradation formed naturally during operation. Therefore, there was no ultraviolet sterilization in the raw tank. Operation parameters and influent water qualities of BEAC and BAC system are summarized in Table 2.

Rapid small-scale column tests (RSSCTs) system

RSSCTs system was established according to the dispersed flow pore surface diffusion model using EBCT and hydraulic loading to describe the adsorption process (Greenwald *et al.* 2015). RSSCTs can obtain breakthrough curves in a fraction of the time with a fraction of water (Sperlich *et al.* 2005). It was consequently employed to quickly quantify adsorption capacities and parameters were summarized in Table 2. Carbon samples were pre-treated as follows: (1) carbons were thoroughly washed with deionized water until all dust was removed and the pH of the wash water was steady; (2) well-washed carbons were dried at 150 °C for 4 h; (3) carbon water slurry was heated to boiling for 30 min and loaded into the column after cooling to room temperature. The feed water qualities were listed in Table 2.

Sampling and analysis

Removal efficiencies of DOC and UV_{254} were determined in pilot-scale and RSSCT system. Three-dimensional

fluorescence spectra (3D-EEM) of water samples were scanned with 5 nm increments by a fluorescence spectrophotometer (FP-6500) (Gong *et al.* 2013). Gas chromatography-mass spectrometry analysis (GC-MS) was performed using chromatography-mass spectrometer (6890GC-5973/5975MSD).

Cumulative uptake of micro-pollutants

The concentration levels of micro-pollutants (DOC) were reported as functions of the operational time and water volume fed to carbon columns divided by mass of GAC (*KBV*). The *KBV* can be described by the following equation:

$$KBV = \frac{V_{\text{Treated}}}{M_{AC}} = \frac{N \cdot Q_{\text{in}}}{1000 \cdot M_{AC}} \tag{9}$$

The *KBV* of pilot-scale system reached up to 39.50 $m^3 \cdot H_2O/(kg \cdot carbon)$ and it was equivalent to 246 days of operation. Performance of micro-pollutants removal from water by carbons in BEAC/BAC and RSSCTs system was also represented by the cumulative uptake DOC (*QC*) as a function of *KBV*.

$$QC = \frac{Q_{\text{in}}}{2M_{AC}} \cdot \sum_{i=1}^{n} \Delta t_i \cdot \begin{bmatrix} (\text{DOC}_{\text{Mn}}^{\text{in},i-1} + \text{DOC}_{\text{Mn}}^{\text{in},i}) \\ -(\text{DOC}_{\text{Mn}}^{\text{out},i-1} + \text{DOC}_{\text{Mn}}^{\text{out},i}) \end{bmatrix} \tag{10}$$

RESULTS

Pore structure distribution

Results of N_2 adsorption/desorption isotherms suggested that MCGL-4/3 obtained remarkable type-IV isotherms with capacities of 815/733 cm^3/g. However, N_2 adsorption capacities achieved by MCGL-2/1 were under 520 cm^3/g. Physico-chemical properties based on N_2 adsorption/desorption isotherms were summarized in Figure 3 and Table 3. As shown in Table 3, total porous volumes (V_{total}) of MCGL-4 and MCGL-3 reached to 1.1688 and 1.0495 cm^3/g, respectively, higher than MCGL-2 (0.8029 cm^3/g) and MCGL-1 (0.7041 cm^3/g). Mesoporous volume (V_{mes}) of MCGL-4 increased to 0.7605 cm^3/g with highest mesoporosity ($V_{\text{mes}}/V_{\text{total}} = 65.11\%$), followed by MCGL-3 (0.6740 cm^3/g, 64.22%). Figure 3(b) furtherly indicated that MCGL-4 had higher pore volume increment (>50 Å) with significant changes in peak value during 50~300 Å. V_{mes} of MCGL-4 was mainly contributed by pore structures during 20.4~52.5 Å (0.2405 cm^3/g), 52.5~208.2 Å (0.4443 cm^3/g) and 208.2~408 Å (0.1225 cm^3/g). MCGL-3 achieved highest micro-porous volume ($V_{\text{micro}} = 0.2900$ cm^3/g) and micro-porous surface area ($S_{\text{Micro}} = 638.42$ m^2/g), followed by MCGL-4 ($V_{\text{micro}} = 0.2655$ cm^3/g and $S_{\text{Micro}} = 588$ m^2/g).

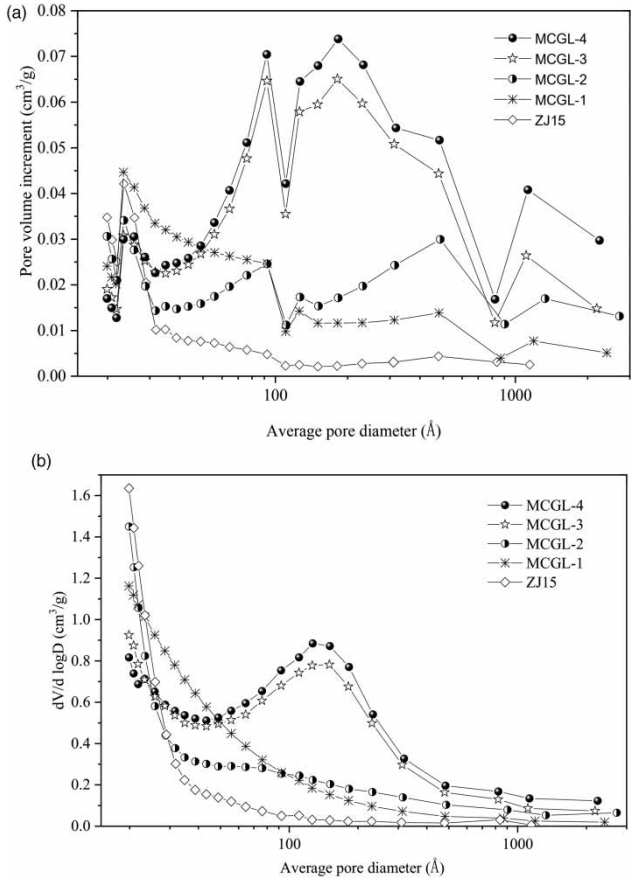

Figure 3 | Physico-chemical properties of new carbons. (a) Distribution of pore size and pore volumes, (b) d*V*/dlog*D*.

Results also suggested that MCGL-3 obtained highest iodine adsorption value (1,185 ± 5.6 mg/g), followed by MCGL-2 (1,062 ± 8.9 mg/g), MCGL-4 (1,110 ± 6.8 mg/g) and MCGL-1 (1,127 ± 7.4 mg/g). However, MCGL-4

Table 3 | Physico-chemical properties of new carbons

		Activated carbons			
Index	**Unit**	**MCGL-4**	**MCGL-3**	**MCGL-2**	**MCGL-1**
S_{BET}	m^2/g	1,265	1,316	1,183	1,090
S_{Ext}	m^2/g	655.41	677.99	705.91	744.94
S_{Micro}	m^2/g	588	638.42	477.51	363.62
V_{total}	cm^3/g	1.1688	1.0495	0.8029	0.7041
V_{micro}	cm^3/g	0.2655	0.2900	0.2368	0.1594
V_{mes}	cm^3/g	0.7605	0.6740	0.3986	0.3502
V_{mar}	cm^3/g	0.1629	0.0855	0.1675	0.1945
D	Å	36.84	32.93	26.12	25.85
Pore volume distributions					
20.4~52.5Å	cm^3/g	0.2405	0.2364	0.2035	0.1648
52.5~208.2Å	cm^3/g	0.4443	0.3979	0.1748	0.1200
208.2~408Å	cm^3/g	0.1225	0.1105	0.0440	0.0335
408~943Å	cm^3/g	0.0685	0.0561	0.0413	0.0224
943~3,000Å	cm^3/g	0.0705	0.0412	0.0300	0.0188

achieved highest properties on methylene blue (251 ± 3.2 mg/g), higher than MCGL-3 (234 ± 4.1 mg/g), MCGL-2 (205 ± 4.3 mg/g) and MCGL-1 (196 ± 1.4 mg/g).

Adsorption capacities of NOM

Adsorption property of humic acid (V_{HA}) was employed to evaluate NOM adsorption. Results suggested that V_{HA} of commercial carbons SX-10, F400 and ZJ15 were 0.626, 0.797 and 0.303 mg/g, respectively. After pore structures regulation, values of V_{HA} of MCGL-4 and MCGL-3 increased to 1.033 and 0.908 mg/g, respectively, higher than MCGL-2 (0.562 mg/g) and MCGL-1 (0.692 mg/g). It also identified that V_{HA} has fine linear correlation with the V_{mes} ($R^2 = 0.9541$) and V_{total} ($R^2 = 0.9293$) based on 7 carbons used in present work. And the corresponding pore volume ($20.4 \sim 208.2$ Å) has the highest linear correlation coefficient with V_{HA} ($R^2 = 0.9830$), followed by pores during $208.2 \sim 408$ Å ($R^2 = 0.9741$), $52.5 \sim 208.2$ Å ($R^2 = 0.9617$) and $20.4 \sim 52.5$ Å ($R^2 = 0.8827$). Therefore, increase of mesoporous volume (MCGL-3 and MCGL-4), especially during the range of $20.4 \sim 208.2$ Å, may well facilitate the adsorption capacities for NOM. Molecular weight distribution of NOM can influence its diffusion rate and adsorbability. Ultrafiltration membrane classification of molecular weight of humic acid was consequently conducted. And relationships between pore distributions and adsorption capacities of humic acid with different ranges of molecular weight were illustrated in Fig S1.

As shown in Fig S1 (a-c), pore volumes during 52.5 to 408 Å was well correlated with adsorption capacity of humic acid ($R^2 > 0.96$), when average molecular weight were below 1,600 *Da*. As mentioned above, pore volumes during 52.5~208.2 Å were much more higher than 208.2~408 Å. Therefore, mesoporous volume during 52.5~208.2 Å may mainly provide surface adsorption site. When average molecular weight increased to 2,700~5,100 *Da* (Fig S1 (d-f), adsorption capacities also increased with the increase of mesoporous volume during 52.5~208.2 Å. However, the linear correlation was not significant. Well linear correlation ($R^2 > 0.96$) was observed during 408~903 Å, it suggested macroporous structure may also play an important role.

Immobilization properties for functional bacteria

Another goal of present work is to improve the properties of bio-enhancement on carbon surface. Studies suggested that initially immobilized biomass of functional bacteria in BEAC process can significantly shorten the biofilm formation, and consequently improve bio-degradation of organic-pollutants. As shown in Fig S2(a), biomass (phospholipid content) on carbons increased over time of cyclic loading. After 24 hours, MCGL-4 obtained 9.13 mmol-P/g of phospholipid content, higher than other 6 carbons. After surface back-washing (5 minutes), phospholipid content on MCGL-4 decreased to 8.06 mmol-P/g. However, it was still higher than other carbons. It indicated that immobilized biomass and stabilities on MCGL-4 were significantly promoted. As shown in Fig S2(b), after 240 hours of continuous culture, MCGL-4 achieved higher phospholipid content (30.36 mmol-P/g), with average growth rate of 2.213 mmol-P/g/d.

Water purification performance of MCGL-4

As mentioned above, it suggested that new carbon MCGL-4 has advantages in NOM adsorption, immobilization capability and biodegradability in BEAC process. Therefore,

MCGL-4 was selected as research target in subsequent studies treating source water from Songhua River.

Changings of DOC

Purification performances of pilot-scale systems were determined under 246 days of operation (KBV = 39.50 $m^3 \cdot H_2O$/(kg·carbon)). Changing curves of DOC in BEAC/BAC system were shown in Figure 4(a).

In pilot-scale BAC system (Figure 4(a)), C-MCGL-4 achieved lower average effluent DOC (1.32 ± 0.70 mg/L) than C-SX-10 (1.82 ± 0.79 mg/L) and C-ZJ15 (2.50 ± 0.72 mg/L). Effluent DOC of C-ZJ15 exceed 3.0 mg/L during KBV ranges of 19.2–39.50 $m^3 \cdot H_2O$/(kg·carbon). However, it remained stable lower level in C-MCGL-4 (2.03 ± 0.15 mg/L) and C-SX-10 (2.58 ± 0.25 mg/L).

In the pilot-scale BEAC system, it indicated that B-MCGL-4 achieved the highest DOC removal efficiency (76% ± 15%) with lowest average value (0.98 ± 0.56 mg/L). Effluent DOC reached a steady state (1.57 ± 0.15 mg/L) after 120 days of operation (19–39.50 $m^3 \cdot H_2O$/(kg·carbon)). However, immobilization did not significantly facilitate the DOC removal in B-ZJ15 (2.34 ± 0.65 mg/L). Removal efficiency of DOC achieved by B-SX-10 increased 12% in comparison with C-SX-10.

3D-EEM And GC-MS spectrometry

The excitation (EX) and emission (EM) boundaries of 3D-EEM were classified into five regions by Chen and Liu *et al.* (Chen *et al.* 2003; Liu *et al.* 2015). Regions-I and -II (EX < 250 nm, EM < 380 nm) associates with aromatic proteins, Region-III (EX < 250 nm, EM > 380 nm) represents fulvic acid-like compounds, Region-IV (EX > 250 nm, EM < 380 nm) represents soluble microbial by-product-like compounds, and Region V (EX > 250 nm, EM > 380 nm) represents humic-like organic compounds. Results of 3D-EEM suggested that the major organic compounds in source water were humic acid-like organics, with two prominent fluorescence peaks (EX/EM = 263 nm/438 nm, EX/EM = 308 nm/423 nm) in Region V. After sand filter purification, the fluorescence intensity decreased slightly.

Figure 4(b) and 4(c) illustrated the average fluorescence intensity during KBV ranges of 5~30 $m^3 \cdot H_2O$/(kg·carbon).

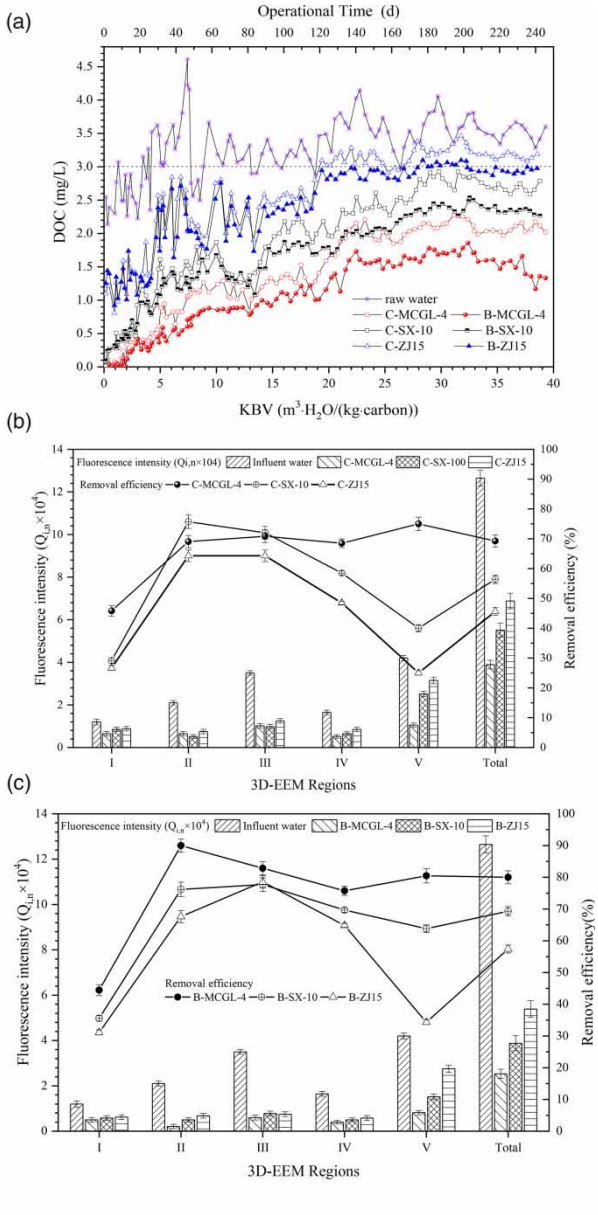

Figure 4 | Water purification performances of carbons in pilot-scale BAC and BEAC system. (a) Changing curves of DOC, (b) change of fluorescence intensity in BAC system, (c) change of fluorescence intensity in BEAC system.

The total intensity of influent water of pilot-scale system was 1.27×10^5, with higher proportion in Region III (fulvic acid-like compounds, 3.5×10^4, 27.56%) and V (humic-like organic compounds, 4.2×10^4, 33.08%). Therefore, removal of fulvic acid- and humic acid-like organics were the core objectives. The total fluorescence intensities (removal

efficacy) of C-MCGL-4、C-SX-10 and C-ZJ15 decreased to 3.89×10^4 (69.25%), 5.51×10^4 (56.44%) and 6.88×10^4 (45.62%), respectively. C-MCGL-4 removed 75% of humic acid-like organics (Region V), followed by 68.49% of fulvic acid (Region IV). It indicated that fulvic acid- and humic acid-like organics can be well removed by new carbon MCGL-4 in BAC system.

In pilot-scale BEAC system, the total fluorescence intensity decreased by 34.96% after bio-enhancement of B-MCGL-4, in comparison with C-MCGL-4. And descend ranges of fluorescence intensities achieved by B-MCGL-4 were 23.08% (Region I), 67.69%(II), 41.18%(III), 23.08%(IV) and 21.90%(V). Therefore, B-MCGL-4 achieved highest removal efficiency for aromatic proteins (Region II and I), followed by fulvic acid-like compounds (Region-III). Moreover, bio-enhancement also improved the removal of soluble microbial by-product-like compounds (Region IV) humic-like organic compounds (Region V) in B-MCGL-4 system.

GC-MS was also used to characterize the purification performances of carbons (at 20 $m^3 \cdot H_2O$/(kg·carbon)). Results suggested that about 101 kinds of organic-pollutants were detected in influent water of pilot-scale system, mainly contains alkanes (30%), benzene compounds (19.7%), naphthalenes (11.1%), olefins (6.2%), and organic ester compounds (4.9%) (Wang *et al.* 2012, 2018). For C-MCGL-4, about 65 kinds of organics were detected, and peak abundance and area decreased sharply during the retention time ranges of 6–12 min and 17–30 min (mainly alkanes, benzene and naphthalene compounds). In BEAC system (B-MCGL-4), peak abundance and area decreased during retention time range of 5–20 min in comparison with C-MCGL-4. The amount of alkanes, benzene and naphthalene compounds decreased by 15.26%, 16.37% and 8.29%, respectively.

Biological proliferation on carbon surface in BEAC system

Biological proliferation on carbon surface in B-MCGL-4 was also determined. The biomass on B-MCGL-4, B-SX-10 and B-ZJ15 reached to 45.6, 34.5 and 28.6 mmol-P/gat 39.50 $m^3 \cdot H_2O$/(kg·carbon).

DISCUSSION

Pore structure regulation mechanisms

The normal distributions of pore structures of 47 kinds of commercial activated carbons (Figure S3) were summarized. New carbon MCGL-4 showed higher levels of V_{total} and V_{mes} than most of carbons, and it also has average level of V_{micro}. It identified that synchronous well-developed mesoporous and micro-porous structures are the most distinguishing characteristics of MCGL-4.

Catalytic carbonization or activation is a promising way to regulate pore structures, and KOH was usually used to promote condensation polymerization and aromatization, so as to form rich micro-porous structures. Martins (Martins *et al.* 2015) pointed that proper amount of KOH impregnation was beneficial for development of micro-porous structure, since KOH can promote the changings of pyrolysis, formatting of initial pore structures and crystallite graphite structures. KOH impregnation was introduced in preparation of MCGL-2, and its V_{total} (0.8029 cm^3/g) and V_{micro} (0.2368 cm^3/g) increased by 14.03% and 48.56%, respectively, compared to MCGL-1. Moreover, mesoporous volume of MCGL-2 (0.3986 cm^3/g) increased by 13.82% in comparison with MCGL-1. That is to say, higher microprous volumes can be attributed to KOH impregnation process, by which mesoporous volumes increased during the collapse of micro-pores by steam activation.

CO_2 activation was employed after carbonization in MCGL-3. Compared to MCGL-2, V_{total} and V_{mes} of MCGL-3 increased by 0.2466 cm^3/g and 0.2754 cm^3/g, respectively. Studies suggested that (Gong *et al.* 2009, 2013) activating agent and time have significant effects on surface physiochemical changes. Especially, surface activation using CO_2 as activator was proved to be more likely to form abundant micro-pores due to its linear molecular structure. The increase of micro-pores attributed by CO_2 activation may offer the potential mesoporous foundation during the subsequent activation. Moreover, pore structure distribution of the intermediate product (M1) after CO_2 activation was also determined. Results suggested that about 0.2024 cm^3/g of microprous volume increased in comparison with MCGL-2. It also interprets the effects of CO_2 activation.

Depth activation at 950 °C was employed in MCGL-4, and it can cause higher ablation rate of carbons. Studies also suggested micro-porous carbon can be commonly obtained with ablation rate below 50%. Mesoporous or macro-porous carbons can be obtained when ablation rate was higher than 70%. Well-developed micro-porous and mesoporous structures may be obtained during ranges of ablation rate of 50–70%. Higher ablation rate of C-GL-4 (68.5% ± 2.30%) was confirmed because of the employment of MDA. In comparison with MCGL-3 (with ablation rate of 55.7% ± 1.80%), depth activation at 980 °C causes collapse of micro-pores, by which V_{total}, V_{mes} and V_{mar} of MCGL-4 increase by 0.1279 cm^3/g, 0.0789 cm^3/g and 0.0774 cm^3/g. However, V_{micro} of MCGL-4 decreased by 0.0284 cm^3/g because of the collapse of micro-pores during depth activation.

One objective of present work aims at improving adsorption kinetics and capacities for NOM by pore structure regulation. Results of 3D-EEM and V_{HA} identified that higher mesoporosity (65.11%) and BJH-V_{mes} (0.7605 cm^3/g) of MCGL-4 resulted in accelerating kinetics and capacity for humic-like organics (Kalkan *et al.* 2011; Lu *et al.* 2014; Gong *et al.* 2015a; Greenwald *et al.* 2015). Figure S4 suggested that adsorption of humic acids by MCGL-4/3 followed pseudo-second-order kinetics ($R^2 > 0.998$) when average molecular weight ranged from 2,700 to 5,100 *Da*. It indicated that a key step of velocity control was the adsorption reaction stage, rather than pore diffusion stage. However, adsorption process achieved by MCGL-2/1 followed Weber-Morris kinetic model ($R^2 > 0.998$), and it indicated that adsorption process was mainly influenced by the diffusion of adsorbents in the pores of the adsorbents. The adsorption kinetics results confirmed that mesoporous regulation during 20.4~408 Å promoted adsorption capacities and kinetics.

Comprehensive quantitative indicators of carbons

Selecting or tailoring an excellent carbon for bio-enhancement is a complex process, especially when the pilot-scale or production experimental data were scarce. Lots of factors can influence the carbon selection such as raw water quality, biomass, bio-activities and parameters of filtration, etc. Therefore, methods which can be used to prejudge properties of carbons based on physical and chemical characteristics are of extraordinary value. Under relatively steady operation mode, the key factors of BEAC process were biomass and bio-activities, especially the initial immobilization capacity of biomass (BI). It determined the extent and efficacy of bio-degradation in initial and stably BEAC process. In order to evaluate the BI by different carbons with different PSD/PVD distribution, 'Comprehensive Quantitative Indicators (*CQI*)' was proposed.

Figure 5(a) firstly calculated the linear correlation coefficients (R^2) between initially immobilized biomass (*BI*, 24 h) and parameters of seven carbons used in present work. Linear fitting results identified that orders of correlation coefficient ($R^2 > 0.800$) were as followed: $V_{mes}(0.9827) > V_{HA}(0.9692) > D(0.948) > V_{total}(0.9323) > V_{MB}(0.8896) >$ *oxygen content* $(0.8221) > V_{micro}(0.0011)$. It confirmed that functional bacteria immobilization was significantly influenced by mesoporous structures, adsorption capacities of NOM and surface oxygen content. While V_{micro} had little correlation, and it also explained the deficiency of micro-porous carbons.

An Ideal Model of Carbons for BEAC process (IMC_{BEAC}) was proposed in the present work. Parameters of IMC_{BEAC} were assigned as follows: $S_{BET} \geq 1{,}400\ m^2/g$, $V_{total} \geq 1.90\ cm^3/g$, $V_{micro} \geq 0.60\ cm^3/g$, $V_{mes} \geq 1.00\ cm^3/g$, $V_{mar} \geq 0.25\ cm^3/g$, $D \geq 40$ Å, $V_{IN} \geq 1{,}400$ mg/g, $V_{MB} \geq 350$ mg/g, $V_{HA} \geq 2.0$ mg/g, *strength* ≥ 90% and density ≥ 500 g/L. Based on the IMC_{BEAC}, Comprehensive Quantitative Indicators (*CQI*) was proposed consequently to evaluate the initial immobilization capacity of biomass (*BI*) by different carbons. It was identified using Equation (11).

$$CQI = \sum_{i=1}^{n} CQI_i = \sum_{i=1}^{n} \left(W_i \times \frac{V_i}{V_{i-IMC}} \right) \tag{11}$$

Here, V_i was parameters of carbons used in present work (Tables 1 and 3); W_i was the linear correlation coefficients (R^2) in Figure 5(a), $V_{i\text{-}IMC}$ was parameters of IMC_{BEAC} as mentioned above.

As shown in Table 4, the calculated *CQI* of IMC_{BEAC} was 6.97, followed by MCGL-4(5.36)>MCGL-3(4.95)>MCGL-2(4.12)>F400(3.78) = MCGL-1(3.78)>SX-10(3.53)>ZJ15(2.51). Linear correlation analysis between *CQI*

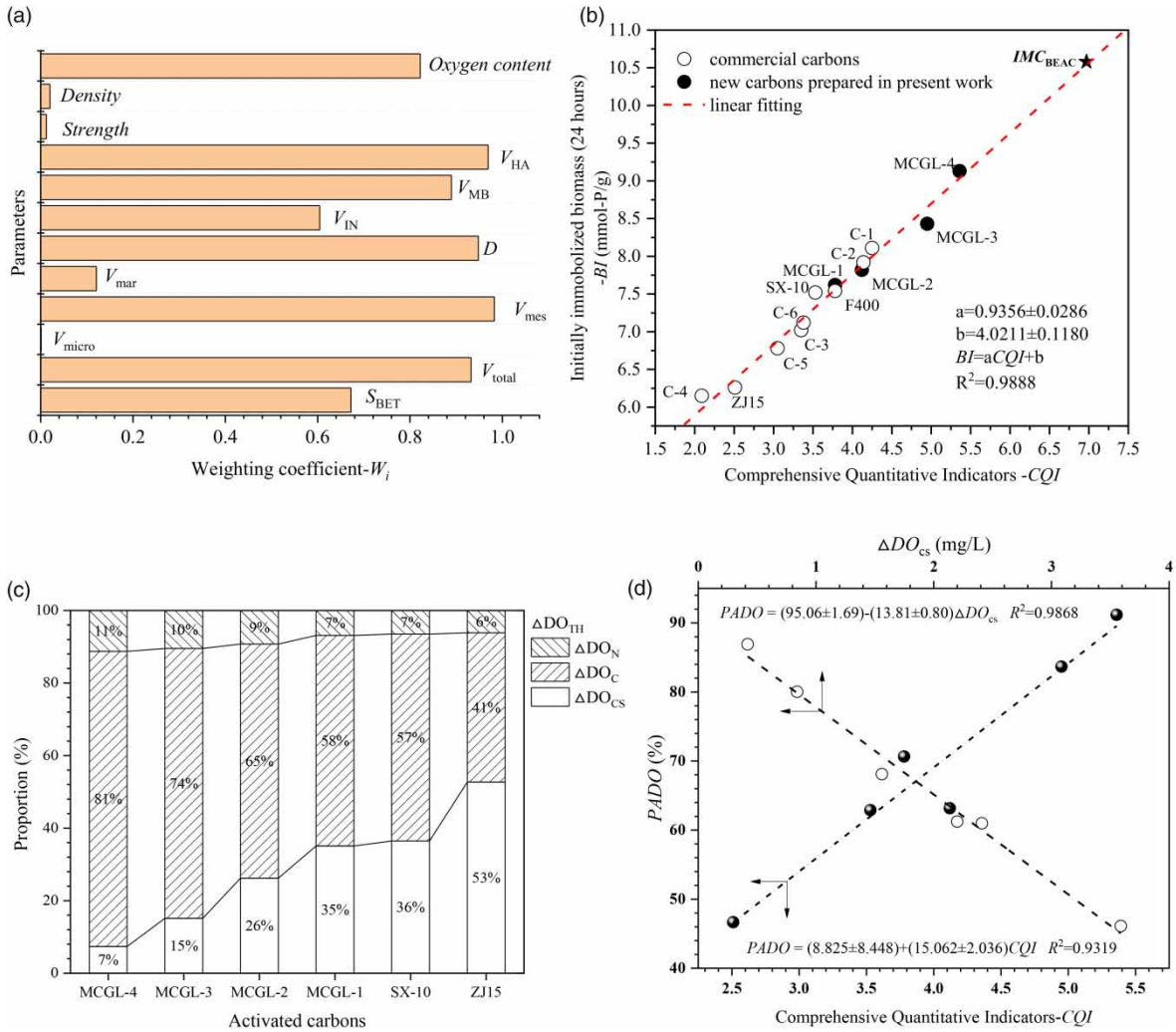

Figure 5 | Comprehensive quantitative Indicators. (a) W_i, (b) linear fitting of *CQI* and *BI*, (c) parameters of bioactivity, (d) linear fitting between *PADO* and *CQI*.

and *BI* was conducted in Figure 5(b), based on 12 tested carbons. Results suggested that initial immobilization capacity of biomass (*BI*) can be well reflected by *CQI* of carbons. According to equations ($BI = 0.9231CQI + 4.0649 (R^2 = 0.9776)$) obtained from Figure 5(b), calculated *BI* of IMC_{BEAC} was 10.499 mmol-P/g. This phenomenon suggested a feasible method to rapidly evaluate the surface immobilization ability of functional bacteria. *CQI* proved to be a promising parameter ($R^2 = 0.9319$) to prejudge *BI* of different carbons. Results of pilot-scale BEAC and BAC system also identified that the selected new carbon MCGL-4 obtained higher efficacy for organics removal and bio-degradation efficiency.

DO consumption and utilization efficiency during bio-degradation

Yapsakli *et al.* (Yapsakli & Cecen 2010; Yapsakli *et al.* 2010) and Aktas & Cecen (Aktas & Cecen 2010) suggested that bio-degradation was closely related to DO consumption and utilization efficiency. Surface affinity for DO was affected by surface oxidation degree. The amount of DO which can be available for bio-degradation decreased with the increase in surface affinity for DO. Surface oxygen content was also proved to be an important factor that can affect the immobilization of functional bacteria ($R^2 = 0.8221$). Therefore, DO consumption and

Table 4 | Comprehensive quantitative indicators (CQI, dimensionless unit)

				Activated carbons												
i	Parameters	W_i	IMC	MCGL-4	MCGL-3	MCGL-2	MCGL-1	SX-10	ZJ15	F400	C-1	C-2	C-3	C-4	C-5	C-6
1	Strength	0.0124	0.01	0.01	0.01	0.01	0.01	0.01	0.01	0.01	0.01	0.01	0.01	0.01	0.01	0.01
2	Density	0.0202	0.02	0.02	0.02	0.02	0.02	0.02	0.02	0.02	0.02	0.02	0.02	0.02	0.02	0.02
3	Oxygen content	0.8221	0.82	0.82	0.74	0.69	0.59	0.54	0.34	0.41	0.60	0.65	0.51	0.35	0.46	0.43
4	S_{BET}	0.6721	0.67	0.60	0.63	0.57	0.52	0.44	0.44	0.56	0.48	0.51	0.44	0.58	0.49	0.60
5	V_{total}	0.9323	0.93	0.58	0.51	0.39	0.35	0.32	0.18	0.44	0.41	0.36	0.27	0.24	0.33	0.27
6	V_{micro}	0.0011	–	–	–	–	–	–	–	–	–	–	–	–	–	–
7	V_{mes}	0.9827	0.98	0.74	0.66	0.39	0.34	0.29	0.04	0.31	0.39	0.34	0.20	0.09	0.15	0.22
8	V_{mar}	0.1207	0.12	0.08	0.04	0.08	0.09	0.06	0.04	0.05	0.03	0.04	0.03	0.01	0.04	0.04
9	D	0.948	0.95	0.90	0.78	0.62	0.61	0.64	0.43	0.69	0.79	0.75	0.66	0.24	0.46	0.58
10	V_{IN}	0.6043	0.60	0.48	0.51	0.49	0.46	0.42	0.41	0.48	0.49	0.44	0.41	0.48	0.47	0.44
11	V_{MB}	0.8896	0.89	0.64	0.59	0.52	0.50	0.48	0.44	0.47	0.61	0.64	0.50	0.02	0.39	0.51
12	V_{HA}	0.9692	0.97	0.50	0.44	0.34	0.27	0.30	0.15	0.34	0.42	0.37	0.29	0.04	0.23	0.27
CQI			6.97	5.36	4.95	3.78	4.12	3.53	2.51	3.78	4.25	4.14	3.35	2.09	3.05	3.38

utilization efficiency during bio-degradation were determined in Figure 5 and Table 5 according to methods described earlier.

As shown in Table 5, considerable differences were observed in surface affinity for DO during adsorption process (ΔDO_{CS}) in column-A. And it indicated that ΔDO_{CS} were negatively correlated with thermal ablation rate of carbons. Fitting results also showed that linear correlation coefficient between ΔDO_{CS} and surface oxygen content was 0.9725. The bio-degradation efficiency of DOC and NH_4^+-N in column B increased with the decrease of ΔDO_{CS}. The theoretical amounts of DO required in bio-degradation of DOC (ΔDO_C) and NH_4^+-N (ΔDO_N) in column B (MCGL-4) were 4.62 ± 0.12 mg/L and 0.64 ± 0.15 mg/L, respectively. The

Table 5 | Parameters relating to DO consumption and utilization during biodegradation

		Activated carbons					
Parameters	unit	MCGL-4	MCGL-3	MCGL-2	MCGL-1	SX-10	ZJ15
DO	mg/L	7.76 ± 0.27	7.65 ± 0.34	7.82 ± 0.26	7.66 ± 0.31	7.69 ± 0.21	7.88 ± 0.13
ΔDO_{CS}	mg/L	0.42 ± 0.07	0.84 ± 0.05	1.56 ± 0.06	2.20 ± 0.06	2.41 ± 0.13	3.59 ± 0.06
ΔDOC_{Bio}	mg/L	1.74 ± 0.06	1.55 ± 0.09	1.45 ± 0.04	1.37 ± 0.12	1.42 ± 0.03	1.05 ± 0.04
ΔN_{Bio}	mg/L	0.15 ± 0.03	0.13 ± 0.03	0.12 ± 0.04	0.10 ± 0.05	0.10 ± 0.04	0.09 ± 0.03
ΔDO_C	mg/L	4.62 ± 0.10	4.13 ± 0.06	3.84 ± 0.11	3.64 ± 0.09	3.77 ± 0.08	2.80 ± 0.11
ΔDO_N	mg/L	0.64 ± 0.15	0.58 ± 0.12	0.55 ± 0.14	0.43 ± 0.06	0.43 ± 0.09	0.42 ± 0.13
ΔDO_{TH}	mg/L	5.69 ± 0.18	5.55 ± 0.13	5.95 ± 0.16	6.28 ± 0.11	6.62 ± 0.12	6.80 ± 0.12
ΔDO_R	mg/L	5.77 ± 0.17	5.62 ± 0.14	6.08 ± 0.17	6.46 ± 0.13	6.69 ± 0.17	6.89 ± 0.10
PADO	%	91.17 ± 0.59	83.67 ± 2.81	70.65 ± 2.28	63.16 ± 3.11	62.89 ± 2.39	46.66 ± 3.49
Ablation rate	%	68.5 ± 2.30	55.70 ± 1.80	49.30 ± 2.70	43.5 ± 3.20	40.15 ± 3.3	33.63 ± 1.8
Oxygen content	%	15.96	9.02	8.45	7.22	6.57	4.12

total theoretical consumption of DO in column B (MCGL-4) ($\Delta DO_{TH} = \Delta DO_C + \Delta DO_N + \Delta DO_{CS}$) was 5.69 ± 0.18 mg/L. As shown in Figure 5(c) (in column B, MCGL-4), percentage occupied by ΔDO_{CS}, ΔDO_C and ΔDO_N were 7, 81 and 11%, respectively. Actual effective utilization rate of DO (*PADO*) by bio-degradation achieved by MCGL-4 in column B reached to 91.17%. In comparison with MCGL-4, micro-porous carbon ZJ15, SX-10 and F400 obtained higher percentage which was occupied by ΔDO_{CS}, rather than bio-degradation of DOC and NH_4^+-N. Therefore, *PADO* was significantly influenced by ΔDO_{CS} ($R^2 = 0.9868$). Moreover, relationship between *PADO* and *CQI* was also determined in Figure 5(d). The fitting results showed that *CQI* was also a promising parameter ($R^2 = 0.9319$) to prejudge *PADO* (bio-activity) of different carbons.

Synergistic efficacy of synchronous adsorption-bio-degradation enhanced by pore regulation

Gibert (Gibert *et al.* 2012), Velten (Velten *et al.* 2011) and Aktaş & Çeçen (Aktaş & Çeçen 2007) pointed out that simultaneous adsorption and bio-degradation were the predominant factors contributing to organic-pollutants removal in BEAC process. The synergistic efficacy of adsorption and bio-degradation can be significantly affected by pore structure regulation (Wang *et al.* 2007; Sulaymon *et al.* 2010). However, it is difficult to quantify the relative contribution rate of the two mechanisms at different operational stages due to lack of methodologies (Oleinikova *et al.* 2018; Schupp *et al.* 2018; Li *et al.* 2019). Cumulative uptake of DOC (*QC*) and RSSCT tests were introduced in present work to quantify synergistic efficacy between adsorption and bio-degradation.

Cumulative uptake of DOC (*QC*)

The changing curves of *QC* calculated from data in Figure 4(a) are illustrated in Figure 6(a) and 6(b). It indicated that *QC* values of pilot-scale BEAC/BAC increased with the extent of operational time/*KBV*. In BAC system (Figure 6(a)), *QC* of C-MCGL-4 reached to 79,614.35 mg·DOC/(kg·carbon) when KBV was 39.50 $m^3 \cdot H_2O$/(kg·carbon) (246 days). While *QC* values of C-SX-10 and C-ZJ15 were 56,539.40 and 28,584.34 mg·DOC/(kg·carbon), respectively. In BEAC system (Figure 6(b)), *QC* obviously increased from the initial stage due to immobilization. *QC* values of B-MCGL-4, B-SX-10 and B-ZJ15 increased to 94,655.50, 67,366.73 and 35,941.86 mg·DOC/(kg·carbon), respectively, at 39.50 $m^3 \cdot H_2O$/(kg·carbon). Well nonlinear fitting ($R^2 > 0.999$) in Figure 6(a) and 6(b) also suggested that *QC* obtained from BAC/BEAC system can be well fitted by nonlinear equation as a function of *KBV*.

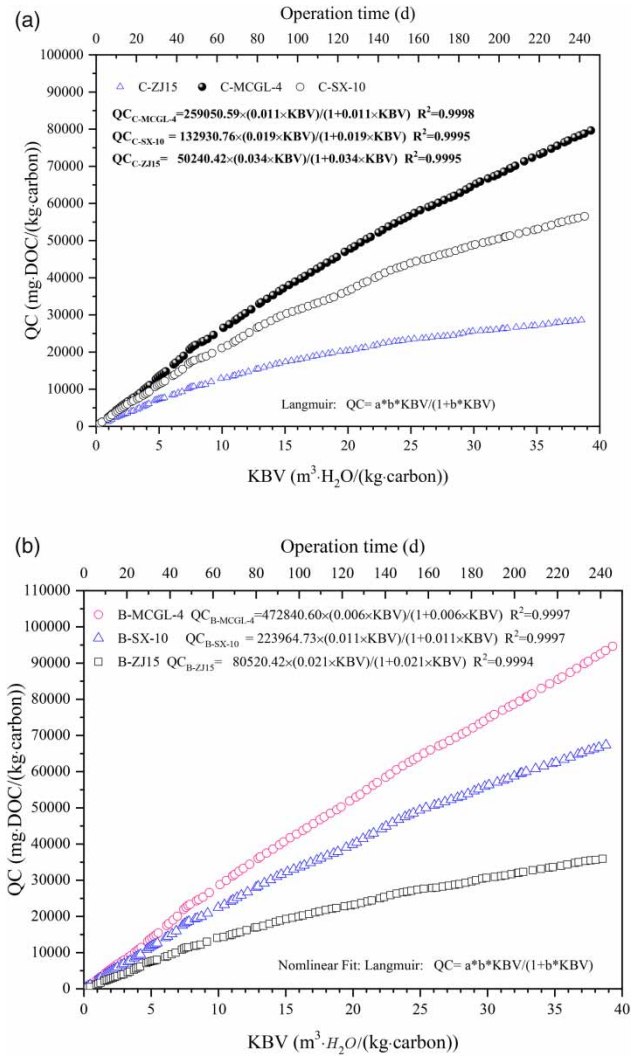

Figure 6 | Cumulative uptake of DOC and related parameters.(a) Pilot-scale BAC system; (b) Pilot-scale BEAC system.

Although it is difficult to directly quantify the relationship between adsorption and bio-degradation, it is clear

that effects of bio-degradation caused by immobilization of functional bacteria in BEAC system can be first evaluated based on data from BAC system. Variable α and β were consequently employed as a function of *KBV*. Variable α is described by the following Equation (12):

$$\alpha_{C-\mathrm{i}} = \frac{QC_{B-\mathrm{i}}}{QC_{C-\mathrm{i}}} \tag{12}$$

Here, parameter i represents carbon MCGL-4, SX-10 or ZJ15. Results suggests $\alpha_{\text{C-MCGL-4}}$ was always higher than 1.0 even at the initial stage of operation; however, it required 3.78 $m^3{\cdot}H_2O/(kg{\cdot}carbon)$ for $\alpha_{\text{C-SX-10}}$ and 3.09 $m^3{\cdot}H_2O/(kg{\cdot}carbon)$ for $\alpha_{\text{C-ZJ15}}$, respectively. It indicated that simultaneous bio-degradation and adsorption occurred in B-MCGL-4 after bacteria immobilization, while B-SX-10 and B-ZJ15 still required a short operational time to achieve effective bio-degradation. The $\alpha_{\text{C-MCGL-4}}$, $\alpha_{\text{C-SX-10}}$ and $\alpha_{\text{C-ZJ15}}$ were 1.184, 1.192 and 1.257, respectively, at 39.50 $m^3{\cdot}H_2O/(kg{\cdot}carbon)$. However, increment value $\Delta QC_{\text{MCGL-4}}$ $(QC_{B-MCGL-4} - QC_{C-MCGL-4})$ reached to 15,041.16 mg·DOC/(kg·carbon)), and it was obviously higher than $\Delta QC_{\text{SX-10}}$($QC_{B-SX-10} - QC_{C-SX-10} =$ 10,827.33 mg·DOC/(kg·carbon)$^-$) and ΔQC_{ZJ15} $(QC_{B-ZJ15} - QC_{C-ZJ15} = 7{,}357.52$ mg·DOC/(kg·carbon)).

Synergy effect between bio-degradation and adsorption

RSSCTs have been widely employed as an established way to accurately predict removal of numerous trace organic chemicals via adsorption to GAC by utilizing pilot-scale columns and thus minimize removal via bio-degradation (Anumol *et al.* 2015). Therefore, cumulative uptake of DOC calculated from the RSSCTs system was compared to results from a BEAC/BAC filter operated in parallel to determine the relative contribution of biodegradation (illustrated in Figure 7(a)) (Zhiteneva *et al.* 2020).

Results suggested that RSSCT-calculated QC can be well nonlinearly represented by RSSCT-calculated KBV ($R^2 > 0.997$). R-MCGL-4 achieved highest capacity (67,725.32 mg·DOC/(kg·carbon)) at 61.40 $m^3{\cdot}H_2O/(kg{\cdot}carbon)$, and 63,175.79 mg·DOC/(kg·carbon)) at 39.50 $m^3{\cdot}H_2O/(kg{\cdot}carbon)$.

Under the assumption above, $\Delta RQC_{\text{B-MCGL-4}}$, $\Delta RQC_{\text{B-SX-10}}$ and $\Delta RQC_{\text{C-MCGL-4}}$ were defined in Equations (13)–(15).

$$\Delta RQC_{B-MCGL-4} = (QC_{B-MCGL-4} - QC_{R-MCGL-4})_{39.5KBV} \tag{13}$$

$$\Delta RQC_{B-SX-10} = (QC_{B-SX-10} - QC_{R-SX-10})_{39.5KBV} \tag{14}$$

$$\Delta RQC_{C-MCGL-4} = (QC_{C-MCGL-4} - QC_{R-MCGL-4})_{39.5KBV} \tag{15}$$

When RSSCT-calculated KBV were 39.50 $m^3{\cdot}H_2O/(kg{\cdot}carbon)$), the calculated $\Delta RQC_{\text{B-MCGL-4}}$, $\Delta RQC_{\text{B-SX-10}}$

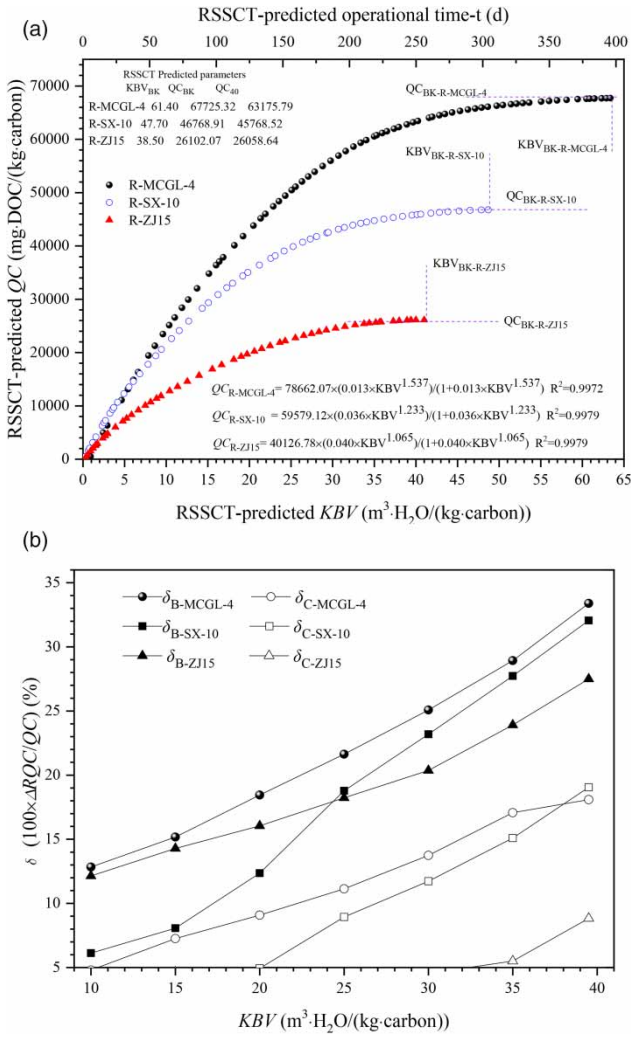

Figure 7 | Variation of the RSSCT-predicted parameters. (a) Variation of RSSCT-predicted *QC*, (b) variation of δ.

and $\Delta RQC_{C\text{-}MCGL\text{-}4}$ were 31,674.72, 21,598.21 and 16,963.54 mg·DOC/(kg·carbon), respectively. It identified that B-MCGL-4 achieved highest bio-degradation abilities. Parameter δ ($100*\Delta RQC/QC$) can be consequently used to represent the contributions of bio-degradation in either BEAC or BAC process for DOC removal.

$$\delta_{B-i}(\%) = 100 \times \frac{\Delta RQC_{B-i}}{QC_{B-i}} \quad (i \text{ was MCGL-4, SX-10 or ZJ15})$$
$$\delta_{C-i}(\%) = 100 \times \frac{\Delta RQC_{C-i}}{QC_{C-i}} \tag{16}$$

As shown in Figure 7(b), $\delta_{B\text{-}MCGL\text{-}4}$ was always higher than $\delta_{B\text{-}SX\text{-}10}$ and $\delta_{B\text{-}ZJ15}$ in BEAC system. The $\delta_{B\text{-}MCGL\text{-}4}$ increased from 12.83% to 33.39% with the extent of KBV, while $\delta_{B\text{-}SX\text{-}10}$ and $\delta_{B\text{-}ZJ15}$ ranged during 6.13~32.06% and 12.14~27.49%, respectively. Moreover, $\delta_{B\text{-}SX\text{-}10}$ was lower than $\delta_{B\text{-}ZJ15}$ during KBV ranges of 10–24 $m^3 \cdot H_2O$/(kg·carbon), it may be attributed to higher adsorption efficiency for DOC by carbon SX-10. However, biological activities were slight ($\delta < 5\%$) in C-SX-10 (KBV < 20 $m^3 \cdot H_2O$/(kg·carbon)) and C-ZJ15 (KBV < 33 $m^3 \cdot H_2O$/(kg·carbon)). δ_c obtained from C-MCGL-4, C-SX-10 and C-ZJ15 increased to 18.08%, 17.05% and 8.84%, respectively, at 39.50 $m^3 \cdot H_2O$/(kg·carbon). Therefore, bio-degradation in B-MCGL-4 accounted for the highest percentages in DOC removal than B-SX-10, B-ZJ15 and BAC process.

CONCLUSIONS

New carbon MCGL-4, tailored by KOH impregnation and MDA, obtained synchronously well-developed meso- (0.7605 cm^3/g), micro- (0.2655 cm^3/g) and macro-porous (0.143 cm^3/g) structures. Mesoporous regulation of MCGL-4 resulted in the promotion of both NOM adsorption and initially immobilized biomass/bio-activity. Mesoporous structure during 20.4~208.2 Å played the most important role in the promotion of adsorption kinetics and capacity for humic-like organics, followed by 208.2~408 Å. Comprehensive Quantitative Indicators of Carbons (*CQI*) was proved to be a promising parameter to prejudge the initial immobilized biomass and bio-activity of different carbons. A new methodology is proposed to quantify the relative contribution rate of adsorption and bio-degradation based on cumulative uptake of DOC (*QC*) in RSSCTs tests system and pilot-scale BEAC system. *QC* achieved by B-MCGL-4 reached to 94,850.51 mg·DOC/(kg·carbon) at 39.50 $m^3 \cdot H_2O$/(kg·carbon). Based on the RSSCTs-calculated cumulative adsorption of DOC, bio-degradation abilities achieved by MCGL-4 in BEAC system reached up to 31,674.70 mg·DOC/(kg·carbon)).

ACKNOWLEDGEMENTS

This study was supported by the Natural Science Foundation of China (NSFC) (Funding No.51708162, 51608149) and Young Innovative Talents Training Program of Heilongjiang Regular Undergraduate Institutions of Higher Learning (Funding No.UNPYSCT-2018131). The authors also thank Harbin Institute of Technology (HIT) and Shanxi Xinhua Chemical Co., Ltd., in the preparation phases of activated carbons.

COMPLIANCE WITH ETHICAL STANDARDS

The manuscript is the original work of authors and it has not been previously submitted to *Water Supply* or other journals for simultaneous consideration. The manuscript has not been published previously. This study is not split up into several parts to increase the number of submissions and submitted to various journals or to one journal over time. No data have been fabricated or manipulated (including images) to support conclusions. No data, text, or theories by others are presented as if they were the author's own. All authors mutually agree for its submission to *Water Supply*. The publication is approved by all authors and tacitly or explicitly by the responsible authorities where the work was carried out.

DATA AVAILABILITY STATEMENT

All relevant data are included in the paper or its Supplementary Information.

REFERENCES

Aktaş, Ö. & Çeçen, F. 2007 Bioregeneration of activated carbon: a review. *Int Biodeterior Biodegradation* **59** (4), 257–272.

Aktas, O. & Cecen, F. 2010 Adsorption and cometabolic bioregeneration in activated carbon treatment of 2-nitrophenol. *J Hazard Mater* **177** (1–3), 956–961.

Al-Amrani, W. A., Lim, P. E., Seng, C. E. & Ngah, W. S. 2012 Bioregeneration of mono-amine modified silica and granular activated carbon loaded with Acid Orange 7 in batch system. *Bioresour Technol* **118**, 633–637.

Anumol, T., Sgroi, M., Park, M., Roccaro, P. & Snyder, S. A. 2015 Predicting trace organic compound breakthrough in granular activated carbon using fluorescence and UV absorbance as surrogates. *Water Res* **76** (0), 76–87.

Chen, W., Westerhoff, P., Leenheer, J. A. & Booksh, K. 2003 Fluorescence excitation-emission matrix regional integration to quantify spectra for dissolved organic matter. *Environ Sci Technol* **37** (24), 5701–5710.

Choi, S. W., Kim, S. & Jung, Y. 2015 Dynamic heterogeneity in crossover spin facilitated model of supercooled liquid and fractional Stokes-Einstein relation. *J Chem Phys* **142** (24), 244506.

Gao, Y. N., Li, W. G., Zhang, D. Y. & Wang, G. Z. 2010 Bio-enhanced activated carbon filter with immobilized microorganisms for removing organic pollutants in the Songhua River. *Water Sci Technol* **62** (12), 2819–2828.

Gibert, O., Lefevre, B., Fernandez, M., Bernat, X., Paraira, M., Calderer, M. & Martinez-Llado, X. 2012 Characterising biofilm development on granular activated carbon used for drinking water production. *Water Res* **47**, 1101–1110.

Gong, G.-z., Xie, Q., Zheng, Y.-f., Ye, S.-f. & Chen, Y.-f. 2009 Regulation of pore size distribution in coal-based activated carbon. *New Carbon Materials* **24** (2), 141–146.

Gong, X., Li, W., Wang, K. & Hu, J. 2013 Study of the adsorption of Cr(VI) by tannic acid immobilised powdered activated carbon from micro-polluted water in the presence of dissolved humic acid. *Bioresour Technol* **141**, 145–151.

Gong, X.-J., Li, W.-G., Wang, G.-Z., Zhang, D.-Y., Fan, W.-B. & Yin, Z.-D. 2015a Characterization and performance evaluation of an innovative mesoporous activated carbon used for drinking water purification in comparison with commercial carbons. *Environ Sci Pollut Res* **22** (17), 13291–13304.

Gong, X.-J., Li, W.-G., Zhang, D.-Y., Fan, W.-B. & Zhang, X.-R. 2015b Adsorption of arsenic from micro-polluted water by an innovative coal-based mesoporous activated carbon in the presence of co-existing ions. *Int Biodeterior Biodegradation* **102**, 256–264.

Gong, X.-J., Li, Y.-S., Dong, Y.-Q. & Li, W.-G. 2020 Arsenic adsorption by innovative iron/calcium in-situ-impregnated mesoporous activated carbons from low-temperature water and effects of the presence of humic acids. *Chemosphere* **250**, 126275.

Greenwald, M. J., Redding, A. M. & Cannon, F. S. 2015 A rapid kinetic dye test to predict the adsorption of 2-methylisoborneol onto granular activated carbons and to identify the influence of pore volume distributions. *Water Res* **68** (0), 784–792.

Haluszka, D., Lorincz, K., Molnar, G., Tamas, G., Kolonics, A., Szipocs, R., Karpati, S. & Wikonkal, N. M. 2015 In vivo second-harmonic generation and ex vivo coherent anti-stokes raman scattering microscopy to study the effect of obesity to fibroblast cell function using an Yb-fiber laser-based CARS extension unit. *Microsc Res Tech* **78** (9), 823–830.

Kalkan, Ç., Yapsakli, K., Mertoglu, B., Tufan, D. & Saatci, A. 2011 Evaluation of biological activated carbon (BAC) process in wastewater treatment secondary effluent for reclamation purposes. *Desalination* **265** (1–3), 266–273.

Li, W., Gong, X., Li, X., Zhang, D. & Gong, H. 2012 Removal of Cr(VI) from low-temperature micro-polluted surface water by tannic acid immobilized powdered activated carbon. *Bioresour Technol* **113**, 106–113.

Li, W. G., Gong, X. J., Wang, K., Zhang, X. R. & Fan, W. B. 2014 Adsorption characteristics of arsenic from micro-polluted water by an innovative coal-based mesoporous activated carbon. *Bioresour Technol* **165**, 166–173.

Li, Q., Lu, H., Yin, Y., Qin, Y., Tang, A., Liu, H. & Liu, Y. 2019 Synergic effect of adsorption and biodegradation enhance cyanide removal by immobilized Alcaligenes sp. strain DN25. *J Hazard Mater* **364**, 367–375.

Liu, X., Yang, Q., Chen, W., Mo, L., Chen, S., Kang, J. & Song, X. 2015 A ratiometric fluorescent probe for rapid, sensitive and selective detection of sulfur dioxide with large Stokes shifts by single wavelength excitation. *Org Biomol Chem* **13** (32), 8663–8668.

Lu, X., Jiang, J., Sun, K., Wang, J. & Zhang, Y. 2014 Influence of the pore structure and surface chemical properties of activated carbon on the adsorption of mercury from aqueous solutions. *Mar Pollut Bull* **78** (1–2), 69–76.

Martins, A. C., Pezoti, O., Cazetta, A. L., Bedin, K. C., Yamazaki, D. A. S., Bandoch, G. F. G., Asefa, T., Visentainer, J. V. & Almeida, V. C. 2015 Removal of tetracycline by NaOH-activated carbon produced from macadamia nut shells: kinetic and equilibrium studies. *Chem Eng J* **260** (0), 291–299.

Oleinikova, O. V., Shirokova, L. S., Drozdova, O. Y., Lapitskiy, S. A. & Pokrovsky, O. S. 2018 Low biodegradability of dissolved organic matter and trace metals from subarctic waters. *Sci Total Environ* **618**, 174–187.

Piai, L., Blokland, M., van der Wal, A. & Langenhoff, A. 2020 Biodegradation and adsorption of micropollutants by biological activated carbon from a drinking water production plant. *J Hazard Mater* **388**, 122028.

Praetorius, S. & Voigt, A. 2015 A Navier-Stokes phase-field crystal model for colloidal suspensions. *J Chem Phys* **142** (15), 154904.

Quinlivan, P. A., Li, L. & Knappe, D. R. 2005 Effects of activated carbon characteristics on the simultaneous adsorption of aqueous organic micropollutants and natural organic matter. *Water Res* **39** (8), 1663–1673.

Schupp, T., Austin, T., Eadsforth, C. V., Bossuyt, B., Shen, S. M. & West, R. J. 2018 A review of the environmental degradation, ecotoxicity, and bioaccumulation potential of the low molecular weight polyether polyol substances. *Rev Environ Contam Toxicol* **244**, 53–111.

Singh, S. K., Townsend, T. G., Mazyck, D. & Boyer, T. H. 2012 Equilibrium and intra-particle diffusion of stabilized landfill leachate onto micro- and meso-porous activated carbon. *Water Res* **46** (2), 491–499.

Smolin, S., Kozyatnyk, I. & Klymenko, N. 2020 New approach for the assessment of the contribution of adsorption, biodegradation and self-bioregeneration in the dynamic process of biologically active carbon functioning. *Chemosphere* **248**, 126022.

Sperlich, A., Werner, A., Genz, A., Amy, G., Worch, E. & Jekel, M. 2005 Breakthrough behavior of granular ferric hydroxide (GFH) fixed-bed adsorption filters: modeling and experimental approaches. *Water Res* **39** (6), 1190–1198.

Spiesshofer, J., Heinrich, J., Lehmann, R., Efken, C., Fox, H., Bitter, T., Korber, B., Horstkotte, D. & Oldenburg, O. 2015 Respiratory effects of adaptive servoventilation therapy in patients with heart failure and Cheyne-Stokes respiration compared to healthy volunteers. *Respiration* **89** (5), 374–382.

Sulaymon, A. H., Ali, A. F. M. & Al-Naseri, S. K. 2010 Mathematical models application for natural organic matter adsorption onto activated carbon. *Desalination Water Treat* **24** (1–3), 93–100.

Ti, Q., Gu, C., Cai, J., Fan, X., Zhang, Y., Bian, Y., Sun, C. & Jiang, X. 2020 Understanding the role of bacterial cellular adsorption, accumulation and bioavailability regulation by biosurfactant in affecting biodegradation efficacy of polybrominated diphenyl ethers. *J Hazard Mater* **393**, 122382.

Velten, S., Boller, M., Koster, O., Helbing, J., Weilenmann, H. U. & Hammes, F. 2011 Development of biomass in a drinking water granular active carbon (GAC) filter. *Water Res* **45** (19), 6347–6354.

Wang, X. 2016 Population balance modeling of precipitated calcium carbonate (PCC) flocculation induced by cationic starches. *Int J Miner Process* **148**, 9–14.

Wang, H., Ho, L., Lewis, D. M., Brookes, J. D. & Newcombe, G. 2007 Discriminating and assessing adsorption and biodegradation removal mechanisms during granular activated carbon filtration of microcystin toxins. *Water Res* **41** (18), 4262–4270.

Wang, H., Jahandar Lashaki, M., Fayaz, M., Hashisho, Z., Philips, J. H., Anderson, J. E. & Nichols, M. 2012 Adsorption and desorption of mixtures of organic vapors on beaded activated carbon. *Environ Sci Technol* **46** (15), 8341–8350.

Wang, H., Qu, B., Liu, H., Ding, J. & Ren, N. 2018 Analysis of organochlorine pesticides in surface water of the Songhua river using magnetoliposomes as adsorbents coupled with GC-MS/MS detection. *Sci Total Environ* **618**, 70–79.

Yapsakli, K. & Cecen, F. 2010 Effect of type of granular activated carbon on DOC biodegradation in biological activated carbon filters. *Process Biochem* **45** (3), 355–362.

Yapsakli, K., Mertoglu, B. & Çeçen, F. 2010 Identification of nitrifiers and nitrification performance in drinking water biological activated carbon (BAC) filtration. *Process Biochem* **45** (9), 1543–1549.

Zhang, D., Li, W., Zhang, S., Liu, M., Zhao, X. & Zhang, X. 2011 Bacterial community and function of biological activated carbon filter in drinking water treatment. *Biomed Environ Sci* **24** (2), 122–131.

Zhiteneva, V., Ziemendorf, E., Sperlich, A., Drewes, J. E. & Hubner, U. 2020 Differentiating between adsorption and biodegradation mechanisms while removing trace organic chemicals (TOrCs) in biological activated carbon (BAC) filters. *Sci Total Environ* **743**, 140567.

First received 25 May 2020; accepted in revised form 22 October 2020. Available online 4 November 2020